

Ionic-Liquid-Doped Polyaniline Inverse Opals: Preparation, Characterization, and Application for the Electrochemical Impedance Immunoassay of Hepatitis B Surface Antigen

By Xing-Hua Li, Lin Dai, Yan Liu, Xiao-Jun Chen, Wei Yan, Li-Ping Jiang,* and Jun-Jie Zhu*

A 3D ordered macroporous (3DOM) ionic-liquid-doped polyaniline (IL-PANI) inverse opaline film is fabricated with an electropolymerization method and gold nanoparticles (AuNPs) are assembled on the film by electrostatic adsorption, which offers a promising basis for biomolecular immobilization due to its satisfactory chemical stability, good electronic conductivity, and excellent biocompatibility. The AuNP/IL-PANI inverse opaline film could be used to fabricate an electrochemical impedance spectroscopy (EIS) immunosensor for the determination of Hepatitis B surface antigen (HBsAg). The concentration of HBsAg is measured using the EIS technique by monitoring the corresponding specific binding between HBsAg and HBsAb (surface antibody). The increased electron transfer resistance (R_{et}) values are proportional to the logarithmic value of the concentration of HBsAg. This novel immunoassay displays a linear response range between 0.032 pg mL^{-1} and 31.6 pg mL^{-1} with a detection limit of 0.001 pg mL^{-1} . The detection of HBsAg levels in several sera showed satisfactory agreement with those using a commercial turbidimetric method.

1. Introduction

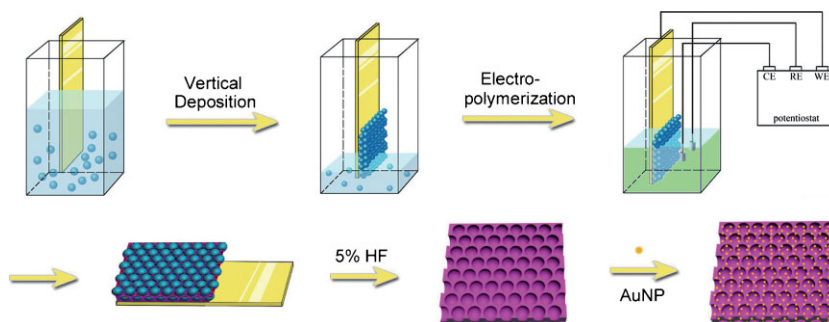
Currently, with the development of nanoscience and nanotechnology, more and more interest has been focused on using assembled nanoparticles to fabricate biosensors.^[1–3] Among these assembled nanostructures, 3D ordered macroporous (3DOM) materials with interconnected macropores (the so-called “inverse opals”) showed potential applications in the field of bioreactors due to their well-designed structures, huge surface area, and unique properties.^[4,5] Self-assembled colloidal crystals, which are close-packed self-assemblies of monodisperse spheres, stand out as ideal templates for 3DOM fabrication by the infiltration of an opal with other materials and subsequent removal of the spheres. Among the

templates, silica with a spherical shape is an ideal candidate material since it can be obtained conveniently in the desired size. Furthermore, commercial silica spheres are available and can be simply removed by dissolution with an aqueous HF solution. So far, various types of inverse opals have been available by utilizing these colloidal crystal templates, for instance, metals,^[4,6–9] inorganic oxides,^[10–12] semiconductors,^[13,14] and polymers.^[15–21] Among these materials, conducting polymers with easily adjustable properties, especially polyaniline (PANI), are much more desirable as inverse opals due to simplicity in the synthesis from an inexpensive monomer, stability in ambient conditions, and unique electrochemical properties such as tunable redox properties.^[22,23]

Recently, some efforts have been made to apply macroporous PANI in the bio-electrochemical field to exploit the advantages provided by the highly ordered porous structure and the huge surface area. Because the PANI obtained by electropolymerization can present a great amount of amine groups with positive charges, it can offer electrostatic anchoring points for nanoparticles or biomolecules with negatively charged surfaces.^[24–27] Meanwhile, because of its favorable storage stability, PANI can act as an immobilization platform for biocomponents. It has been reported that the macroporous PANI is able to electrocatalyze the oxidation of reduced β -nicotinamide adenine dinucleotide (NADH)^[28,29] and catalyze the electrochemical reduction of nitrite,^[30] and it can also be used to fabricate an enzyme electrode for the detection of glucose.^[31] However, PANI does not keep its conductive properties in nonacid media^[32,33] and a neutral condition is required for immunoreactions. The loss of redox activity of PANI in neutral solutions also brings the limitation of using pure PANI inverse opals for immunoassays. As a result, electropolymerization of PANI is preferentially carried out in the presence of dopants. It has been demonstrated that the redox activity of PANI can be sustained in neutral solutions by doping.^[34–36] The inclusion of the dopant maintains electrical neutrality in the oxidized form of the polymer and also leads to an increase in its structural stability and conductivity over a broader range of pH values.

[*] Dr. L.-P. Jiang, Prof. J.-J. Zhu, Dr. X.-H. Li, L. Dai, Y. Liu, Dr. X.-J. Chen, Dr. W. Yan
Key Lab of Analytical Chemistry for Life Science (MOE)
School of Chemistry and Chemical Engineering
Nanjing University
Nanjing, 210093 (P. R.China)
E-mail: Jianglp@nju.edu.cn; jjzhu@nju.edu.cn

DOI: 10.1002/adfm.200901003

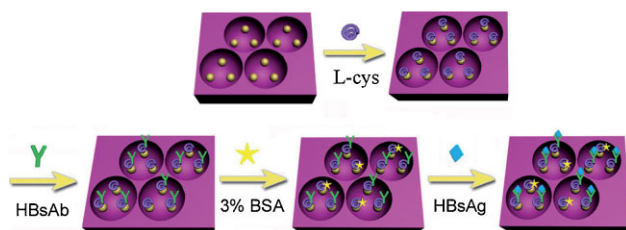


Scheme 1. Procedure for the fabrication of IL-doped PANI inverse opals and self-assembly of AuNPs.

Room temperature ionic liquids (RTILs) have attracted great interest and can be used as new types of dopant in polymer synthesis.^[37–40] RTILs, which are composed of unsymmetrically substituted nitrogen-containing cations (imidazole, pyrrolidine, pyridine, etc.) with inorganic anions (Cl^- , PF_6^- , BF_4^- , etc.), have many unique physicochemical properties, such as high thermal stability, negligible vapor pressure, good electrochemical stability, and conductivity at room temperature.^[41]

Herein, we report an electropolymerization method for the preparation of 3DOM PANI inverse opals doped with 1-butyl-3-methylimidazolium tetrafluoroborate ($\text{BMIm}^+\text{BF}_4^-$) by using silica spheres as the sacrificial template. Citrate-stabilized gold nanoparticles (AuNPs) were assembled on the surface of the 3DOM IL-PANI inverse opals to fabricate the AuNP/IL-PANI composite as shown in Scheme 1. The prepared composite inherited advantages such as good biocompatibility and excellent chemical stability, which made it as an ideal candidate for immunoassays.

As a model, a novel electrochemical impedance spectroscopy (EIS) immunosensor has been developed for the detection of the Hepatitis B surface antigen (HBsAg). Hepatitis B surface antibody (HBsAb) was immobilized on the surface of the AuNP/IL-PANI composite. After blocking with bovine serum albumin (BSA), HBsAg could be detected directly as shown in Scheme 2. The fabricated HBsAg immunosensor exhibited a highly sensitive response to HBsAg with the detection limit of 0.001 pg mL^{-1} , which could be ascribed to the significantly large surface area of the AuNP/IL-PANI composite and the poor conductivity of HBsAg molecules. This material could be further extended to other biological systems because it offers a versatile, practical, and convenient protocol in clinical diagnoses.



Scheme 2. The analytical procedure of HBsAg immunosensing using HBsAb/AuNP/IL-PANI bioconjugates.

2. Results and Discussion

2.1. Preparation and Characterization of the IL-PANI Inverse Opals

2.1.1. SiO_2 Colloidal Templates

The self-assembly of the microspheres is based on the fact that the face-centered-cubic (fcc) structure is a low potential structure regarding mechanical potential energy. Therefore, it is stable and likely to arise from the sedimentation of colloidal suspension of monodisperse microspheres.^[31,42] In our work, with the vertical deposition, highly ordered 3D SiO_2 colloidal assemblies were formed on the gold substrate. Figure 1a and b are scanning electron microscopy (SEM) images of the SiO_2 colloidal crystal template that exhibit a close-packed arrangement of SiO_2 spheres with (111) planes parallel to the substrate surface. In Figure 1a, the hexagonal array structures could be found and the SiO_2 spheres adhered to each other to arrange on the substrate. This good adhesion made the SiO_2 colloidal crystal template a possible candidate for the preparation of IL-PANI inverse opals by electropolymerization. The thickness (number of layers) of the inverse opals could be controlled by changing the condition in vertical deposition and two-layer inverse opals were prepared (Fig. 1b).

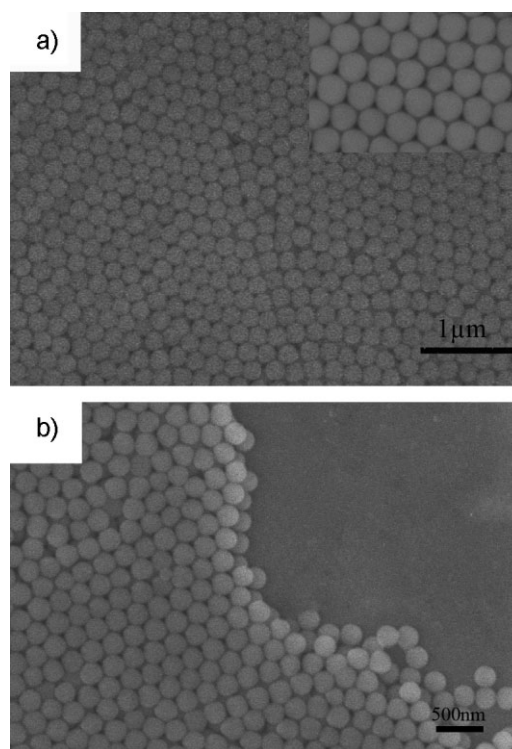


Figure 1. a) Typical SEM images of the SiO_2 colloidal crystal template prepared by vertical deposition. The inset is the image at high magnification of the colloidal crystal. b) Two-layer colloidal crystal observed from the edge.

2.1.2. Fabrication of IL-PANI Inverse Opals

The electropolymerization technique represents a good strategy to synthesize conducting polymer inverse opals because the thickness can be controlled.^[43–45] Electropolymerization also presents some additional advantages for the synthesis, such as easily controllable reaction conditions including the applied potential or time, hypostasis of the dopant or the polymer, etc. Some studies showed that the synthesis of conducting polymers with the electropolymerization could control the quality of the inverse opals, and the method was faster, simpler, and more energy efficient than traditional chemical methods. To the best of our knowledge, there are no reports on the preparation of 3DOM IL-PANI inverse opals by this technique.

IL-PANI inverse opals were fabricated by a potentiostatic technique. After the SiO₂ spheres were removed by diluted HF solution, a well-ordered 3DOM IL-PANI inverse opal was obtained. The self-supporting PANI inverse opal structures were believed to be held together by physical crosslinking and weak interactions such as hydrogen bonding and van der Waals forces between PANI chains.^[45] It can be observed that the IL-PANI appears to be composed of particulates of tens of nanometers according to the SEM (Fig. 2a) and atomic force microscopy (AFM) (Fig. 2b) images. In addition, the enlarged image in Figure 2a shows that the pores

are assembled in a hexagonal arrangement and connected to each other by symmetrical holes, which indicates an inverse opal structure of a continuous 3DOM nature. Compared to chemical polymerization, the quality of IL-PANI inverse opals prepared by the electropolymerization is greatly improved in terms of defect density and structural fidelity of the walls and holes. The center-to-center distance between the pores is (271 ± 12) nm, and the linear shrinkage is about 6.6% with respect to the diameter of the SiO₂ spheres (actually ≈ 290 nm).

By adjusting the quantity of charge in electropolymerization, the potentiostatic technique can be used to control the formation of the IL-PANI inverse opal films. A similar result was also found in the current changes shown in a galvanostatic preparation.^[28] Figure 3a and b show the morphologies of IL-PANI inverse opaline films with different charges. Figure 3a is the SEM image of the film with controlled charge of less than 0.01 C. The diameter of pores is about 200 nm. It can be observed in Figure 3b that some of the pores at the top layer begin to close when the controlled charge is 0.1 C. If the controlled charge of electropolymerization was increased further, all the pores of the top layer were closed. For practical application, an open end of a 3DOM structure similar to Figure 2 was preferred because the large surface area could be obtained in this case. Therefore, we chose the controlled charge of 0.01 C in the present work.

Generally, PANI shows redox activity only in acidic media (pH < 4), which causes the limitation of pure PANI inverse opal application in immunoassays, as neutral conditions are required for immunoreactions. However, the redox activity of PANI can be sustained in neutral pH solutions with doping. The inclusion of the dopant maintains electrical neutrality in the oxidized form of

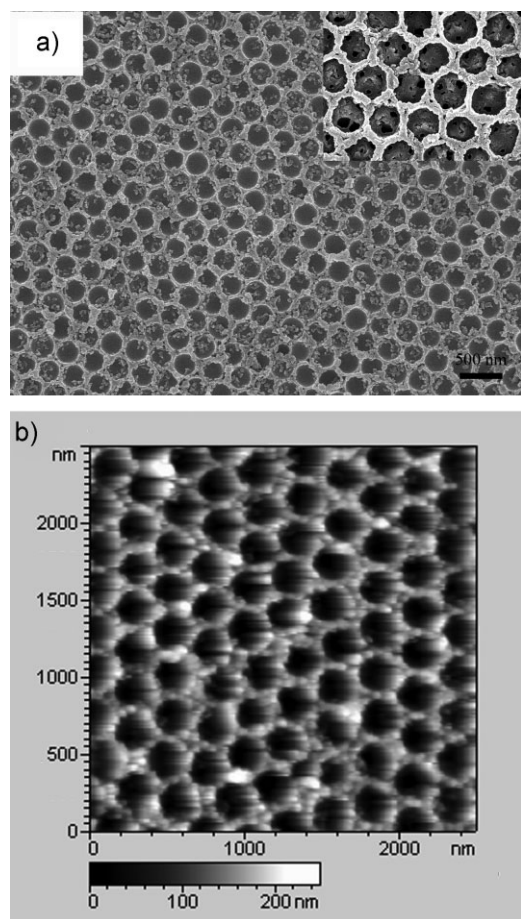


Figure 2. a) SEM and b) AFM images of IL-PANI inverse opals. Inset of (a): enlarged SEM image of IL-PANI inverse opals.

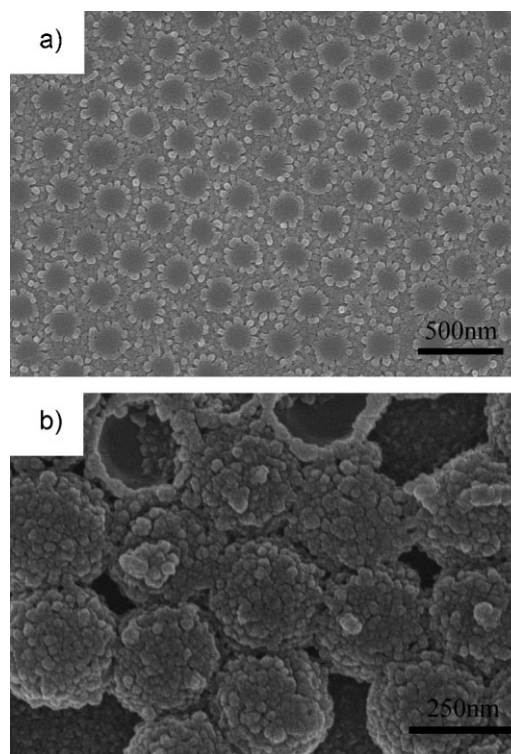


Figure 3. SEM images of IL-PANI inverse opals prepared with a controlled charge of a) less than 0.01 C and b) 0.1 C.

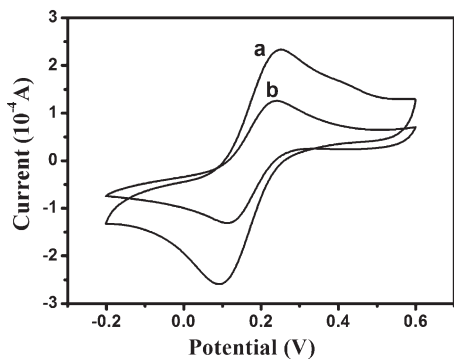


Figure 4. CVs of a) $\text{BMIm}^+\text{BF}_4^-$ doped PANI inverse opals and b) PANI inverse opals without doping in 10 mM pH 7.0 PBS containing 0.1 M KCl and 2 mM $[\text{Fe}(\text{CN})_6]^{3-/4-}$ at 50 mV s^{-1} .

the PANI and also leads to an increase in its conductivity at neutral and even in a broader range of pH values.

$\text{BMIm}^+\text{BF}_4^-$, a kind of RTIL, was used as a dopant during the electropolymerization of aniline, which produced high-quality and well-conducting 3DOM structures. The IL-PANI inverse opal film was electrochemically characterized in 10 mM pH 7.0 phosphate buffered saline (PBS) containing 0.1 M KCl and 2 mM $[\text{Fe}(\text{CN})_6]^{3-/4-}$ at a scan rate of 50 mV s^{-1} as shown in Figure 4, curve a. For comparison, the cyclic voltammogram (CV) of a PANI inverse opal film without any doping is also shown in Figure 4, curve b, which indicates that the amperometric response of the inverse opal film can be influenced by the IL dopant. With IL doping, an obvious increase in the amperometric response was observed, showing that the electron transfer kinetics of $[\text{Fe}(\text{CN})_6]^{3-/4-}$ were enhanced.

2.1.3. Characterization of HBsAb/AuNP/IL-PANI Bioconjugates

For the immobilization of biomolecules in the immunoassay, citrate-stabilized AuNPs were anchored to the surface of the IL-PANI inverse opal film by electrostatic adsorption, which could improve the biocompatibility of the hybrid material and increase the immobilization quantity of biomolecules.^[46] As the IL-PANI inverse opals inherit large numbers of amine groups on the chains of polymer, the positive charge ensures the efficient adsorption with negatively charged AuNPs onto the surface by electrostatic interactions. HBsAb was further immobilized on the surface of AuNP/IL-PANI composites by covalently bonding with L-Cys to form HBsAb/AuNP/IL-PANI bioconjugates for immunoassays. Several experimental techniques were employed to monitor the formation of the HBsAb/AuNP/IL-PANI bioconjugates.

The wetting properties of the material were investigated by measuring the water contact angles (θ) of the inverse opals and

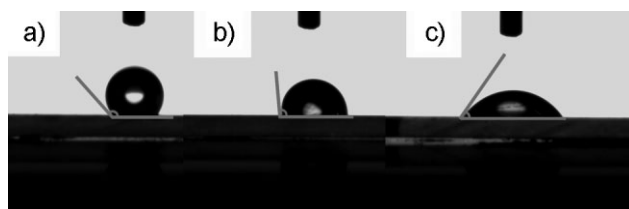


Figure 5. Contact angles of water on a) IL-PANI inverse opals, b) AuNP/IL-PANI composites, and c) HBsAb/AuNP/IL-PANI bioconjugates.

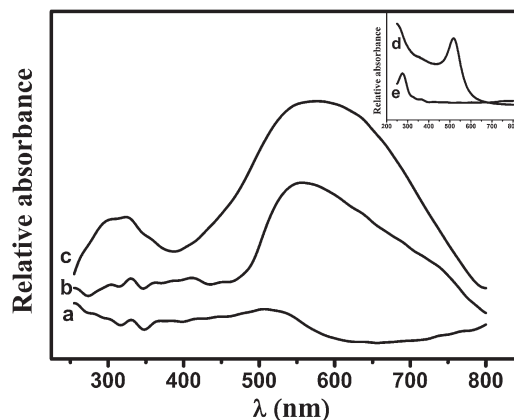


Figure 6. UV-Vis spectra of a) IL-PANI inverse opals, b) AuNP/IL-PANI composites, and c) HBsAb/AuNP/IL-PANI bioconjugates. The insets are UV-Vis spectra of d) AuNPs in solution and e) HBsAb in pH 7.0 PBS.

corresponding composites. Figure 5 compares the contact angles of IL-PANI inverse opals ($\theta = 132^\circ$), AuNP/IL-PANI composites ($\theta = 95^\circ$), and the immobilization of HBsAb ($\theta = 55^\circ$), respectively. It shows that the wettability of material increases significantly with the modified steps. The contact angle decreased from 132° to 95° with absorption of AuNPs, which improved hydrophilicity to the surface and might be helpful for the immobilization of biological molecules. As shown in Figure 5c, after immobilization of HBsAb molecules, the prepared bionic interface with 55° of the contact angle certifies the combination of HBsAb with the AuNP/IL-PANI composites.

UV-Vis spectroscopy has been used to monitor the assembly process. Curve a in Figure 6 is the spectrum of the IL-PANI film after the electropolymerization in which two characteristic absorption peaks of PANI can be observed. The peak at about 330 nm is the $\pi-\pi^*$ transferring peak of benzene ring and the peak at 510 nm is the transferring peak of p bond. After coating with AuNPs, an absorption band between 500 and 750 nm can be observed (Fig. 6, curve b), which is consistent with the surface plasmon resonance of AuNPs. The AuNPs (Fig. 6, curve d) show a strong transverse plasmon band at 513 nm. After AuNPs were adsorbed by IL-PANI inverse opals, the adsorption peak (curve b) became wider than pure AuNPs. This broadening of the bands may be due to the aggregation of AuNPs on the surface of IL-PANI inverse opals. As can be seen in curve c, HBsAb encapsulated in the composite AuNP/IL-PANI inverse opals has a characteristic Soret absorption band at about 310 nm (Fig. 6, curve c), nearly the same as that of native HBsAb in pH 7.0 PBS (curve e), which shows that protein is successfully integrated with the AuNP/IL-PANI composite. On the basis of HBsAb/AuNP/IL-PANI bioconjugates, a novel and sensitive EIS immunosensor has been developed.

2.2. Utilization of Biofunctionalized HBsAb/AuNP/IL-PANI Bioconjugates for Immunoassays

2.2.1. Electrochemical Characteristics of the Electrode Surface

All electrochemical measurements were performed in PBS (pH 7.0) containing 0.1 M KCl and 2 mM $[\text{Fe}(\text{CN})_6]^{3-/4-}$. The

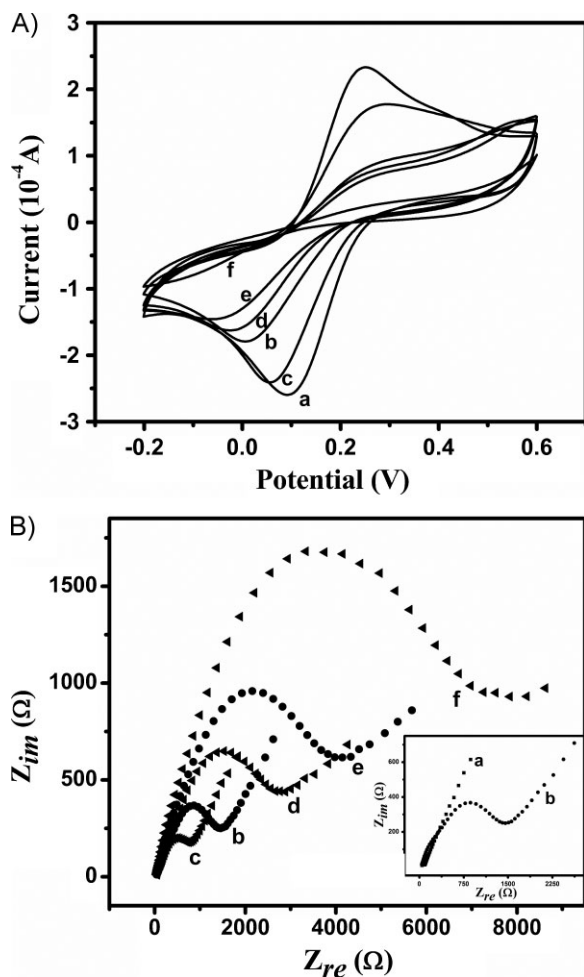


Figure 7. A) CVs and B) EIS images of a modified electrode recorded in PBS (10 mM pH 7.0) solution containing 0.1 M KCl and 2 mM $[\text{Fe}(\text{CN})_6]^{3-/4-}$: a) 3DOM IL-PANI electrode; b) AuNP/IL-PANI electrode; c) L-Cys/AuNP/IL-PANI electrode; d) HBsAb/L-Cys/AuNP/IL-PANI electrode; e) BSA/HBsAb/L-Cys/AuNP/IL-PANI electrode; f) HBsAg/BSA/HBsAb/L-Cys/AuNP/IL-PANI electrode. The scan rate was 50 mV s^{-1} . The inset of (B) is the EIS curve comparison of a) the 3DOM IL-PANI electrode and b) the AuNP/IL-PANI electrode.

ferricyanide was chosen as a marker to investigate the changes of the electrode behavior after each modification step. Figure 7A shows the CVs of $[\text{Fe}(\text{CN})_6]^{3-/4-}$ at different modification steps. When the IL-PANI inverse opals were electropolymerized on the gold substrate, the resulting electrode showed a pair of quasi-reversible redox peaks (Fig. 7A, curve a). By the assembly of AuNPs on the 3DOM IL-PANI electrode surface, an obvious peak current decrease was observed (Fig. 7A, curve b). This may be that the existence of the AuNP layer leads to the increase of film thickness to block the electron transfer kinetics of $[\text{Fe}(\text{CN})_6]^{3-/4-}$.^[47] After L-Cys was functionalized to the AuNP/IL-PANI electrode, the electron transfer between the electrochemical probe and the electrode surface was enhanced (Fig. 7A, curve c) due to the electrostatic attraction of L-Cys with positive charges to the negatively charged electrochemical probe. When HBsAb and BSA were immobilized on the electrode surface in turn, the

peak currents of the redox couple decreased again (Fig. 7A, curve d and e). When HBsAg molecules were combined with the antibody molecules, an obvious disappearance of the redox peaks was observed as shown in Figure 7A, curve f.

EIS is an effective tool for analyzing the changes in the interfaces of modified electrodes in the assembly process.^[48] The advantage of EIS over other electrochemical techniques is that only small-amplitude perturbations from the steady state are needed and information concerning the interface can be provided.^[49] For immunosensors, the $[\text{Fe}(\text{CN})_6]^{3-/4-}$ redox couple is often used to characterize the electrode interface feature in electrochemistry. The electron transfer of $[\text{Fe}(\text{CN})_6]^{3-/4-}$ can be blocked by the formation of antigen–antibody complexes^[43,50–52] on the electrode surface, which results in an increase of the electron transfer resistance. The amount of antigen–antibody complexes is related to the concentration of target antigen in the solution. Here, the formation of HBs antibody–antigen complexes on the resulting electrode was probed by the $[\text{Fe}(\text{CN})_6]^{3-/4-}$ redox couple and monitored by EIS. Figure 7B shows the Nyquist plots of the stepwise modification processes. The 3DOM IL-PANI modified electrode revealed a small semicircle domain (Fig. 7B, curve a), which implied a low-electron-transfer resistance of the redox couple. After the electrode was assembled with AuNPs, the electron transfer resistance (R_{et}) was slightly large (Fig. 7B, curve b), showing that the AuNP layer could inhibit the electron transfer. The L-Cys modified electrode showed a much lower resistance for the redox probe (Fig. 7B, curve c), which implied that the self-assembled layers abundant in amido groups provided a positively charged surface and thus the surface improved the ability of the redox probe to access the layer. Subsequently, the HBsAb molecules were combined on the AuNP/IL-PANI electrode and the R_{et} increased again (Fig. 7B, curve d). The result was consistent with the protein layer on the electrode generating a barrier for electron and mass transfer, and they significantly hindered the diffusion of ferricyanide toward the electrode surface. The resulting electrode was then incubated with BSA and HBsAg molecules (Fig. 7B, curve e and f). Thus the BSA and antigen molecules were successively combined on the surface of the electrode to block the electron transfer.

2.2.2. Optimization of Experimental Conditions

The prepared immunosensor was rinsed with PBS and then incubated in solutions containing different concentration of HBsAg. The HBsAg in solution could be bonded to the electrode surface by the specific antigen–antibody reaction between HBsAg and HBsAb, which could be reflected by the changes in R_{et} values (ΔR_{et}) of the immunosensor. It is well known that the response between antigen and antibody greatly depends on the time and the temperature of incubation. The effects of incubation time and incubation temperature on the reactions were investigated in the PBS containing $[\text{Fe}(\text{CN})_6]^{3-/4-}$ and 0.1 pg mL^{-1} HBsAg.

The effect of incubation time on the EIS response is shown in Figure 8A. It can be seen that ΔR_{et} increased firstly with the increase of reaction time and then reached a plateau after 40 min. The relationship of ΔR_{et} with incubation temperature is shown in Figure 8B and the value of ΔR_{et} increased all along with the temperature rising until a striding point at 60°C , which might be caused by the inactivation of protein molecules at high temperature. The sensor could be used over 37°C without

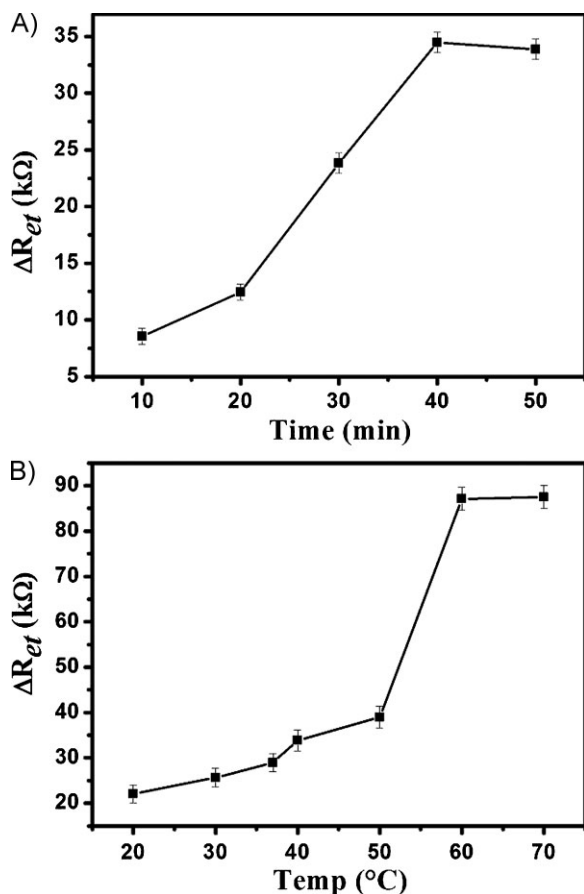


Figure 8. Relationships of ΔR_{et} with the incubation time (A) and incubation temperature (B) on the response of EIS.

irreversible behavior and the result might be attributed to the stability of the 3DOM IL-PANI film and the special heat-resistance properties of HBsAb and HBsAg. Thus, in the present work, 40 min and 50 $^{\circ}$ C were selected as incubation time and temperature, respectively, for the immunoassay of HBsAg.

The size of the SiO₂ spheres played an important role in the pore size of IL-PANI inverse opals, immunoreaction activity, and the immunoassay performance. Figure 9 shows the impedance responses of the AuNP/IL-PANI inverse-opal-modified immunosensors with different template sizes in a 1.0 pg mL⁻¹ HBsAg PBS solution. Among the three electrodes, that electrode with a template size of 250 nm (actually \approx 290 nm) had the highest reaction activity toward the combination of HBsAg. It was observed that the impedance value increased with the decrease of template size since a larger active surface area ratio might immobilize more HBsAb molecules and result in more combinations of HBsAg molecules.

2.2.3. Detection of HBsAg

To evaluate the reaction between antibody and antigen, the sensor with various concentrations of HBsAg (C_{HBsAg}) were fabricated. Before impedance measurements were performed, CV measurements were carried out until the currents were stable. The calibration plot for the determination of HBsAg was obtained with the proposed immunosensor. The corresponding Nyquist plots of

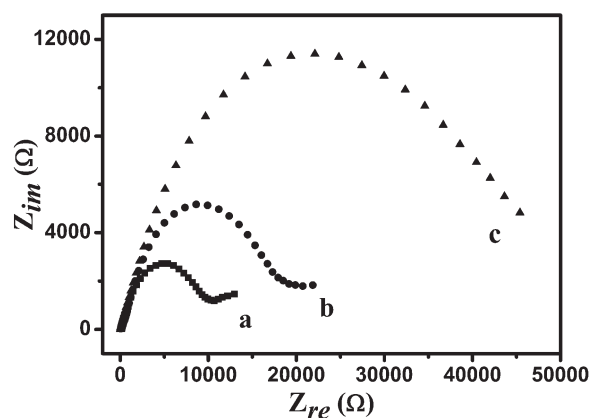


Figure 9. Impedance responses to the same concentration HBsAg (1.0 pg mL⁻¹) PBS solution of AuNP/IL-PANI inverse opal modified electrodes with template sizes of 1 μ m (curve a), 500 nm (curve b), and 250 nm (curve c).

impedance spectra obtained in [Fe(CN)₆]^{3-/4-} solution are shown in Figure 10A. It can be observed that R_{et} increased with the growth of C_{HBsAg} , which may result from more HBsAg molecules bound to the electrode surface blocking the electron transfer. Figure 10B illustrates a linear relationship of ΔR_{et} with the logarithm of C_{HBsAg} in a range from 0.032 to 31.6 pg mL⁻¹ ($r = 0.996$, $n = 7$, where r is the relative coefficient and n is the number). According to the linear equation, HBsAg could be detected. Higher serum HBsAg levels could be detected by an appropriate dilution with pH 7.0 PBS. As can be observed, ΔR_{et} increased with the increase of antigen concentrations within the detection range. However, the increases of ΔR_{et} were not obvious at higher antigen concentrations due to steric hindrance or saturation of coupled antigen molecules.^[53]

Since the isoelectric point (pI) of HBsAg is 4.6, it is negatively charged at pH 7.0,^[54-56] and the electron transfer of the [Fe(CN)₆]^{3-/4-} redox couple can be blocked severely due to the negative charges carried by HBsAg molecules. In addition, the conductivity of HBsAg is poor, and small amounts of HBsAg on the electrode surface result in great changes in EIS responses. Because the AuNP/IL-PANI inverse opals provide a high surface-to-volume ratio, high protein loading could be obtained. As a result, the sensor showed an extremely sensitive response to HBsAg with a detection limit of 0.001 pg mL⁻¹.

2.2.4. Comparison of HBsAg Detection between IL-PANI and PANI

The HBsAg concentration on the basis of PANI inverse opals without IL doping was also detected. A BSA/HBsAb/L-Cys/AuNP/PANI electrode was incubated with equal concentrations of HBsAg at 50 $^{\circ}$ C for 40 min. The response of the sensor with IL-PANI was obviously higher than that without IL doping as shown in Figure 11. The detection range was also broader than that without IL doping. The result indicated that doping with IL played an important role in improving the response for the immunosensor.

2.2.5. Specificity of the Immunosensor

Usually, specificity is an important criterion for immunosensors. In the present study, other proteins such as C-reactive protein (CRP) and immunoglobulin A (IgA) were used to evaluate the

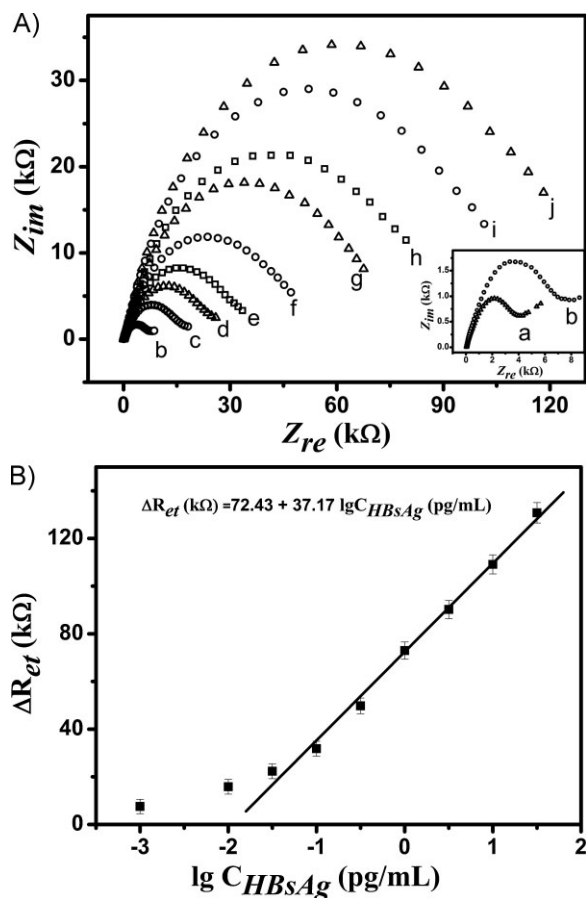


Figure 10. A) Faradaic impedance spectra that correspond to the HBsAg immunosensor before and after incubating with different concentrations of HBsAg in PBS (10 mM pH 7.0) solution containing 0.1 M KCl and 2 mM $[\text{Fe}(\text{CN})_6]^{3-/4-}$: a) blank solution; curves b–j represent 0.001, 0.01, 0.032, 0.1, 0.316, 1.0, 3.16, 10.0, and 31.6 pg mL^{-1} HBsAg, respectively. B) Calibration curve for the HBsAg immunosensor. The inset of (A) is the EIS curve comparison of a) the blank solution and b) 0.001 pg mL^{-1} HBsAg.

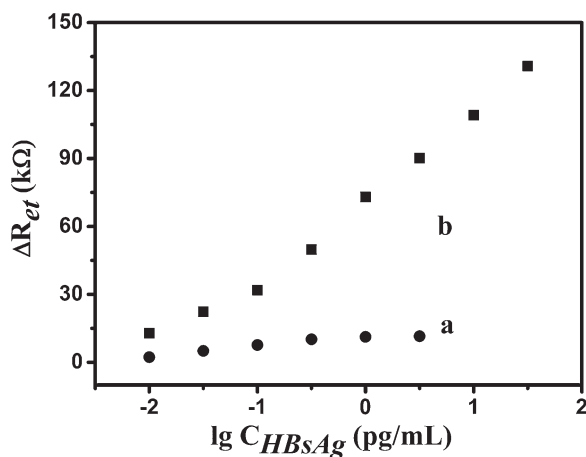


Figure 11. Calibration plots show ΔR_{et} of a) PANI inverse opals without doping as basis and b) IL-doped PANI inverse opals as basis.

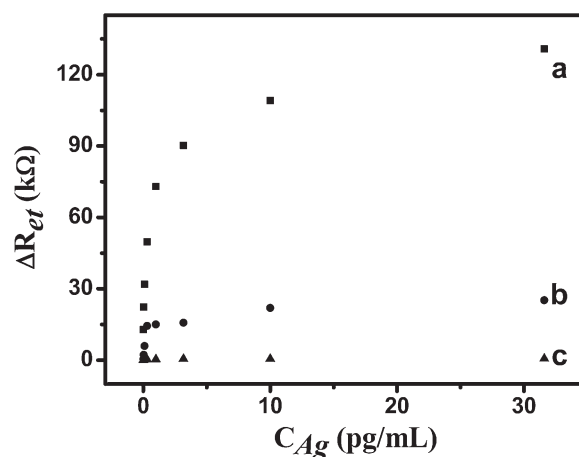


Figure 12. Calibration plots show ΔR_{et} of the different concentrations of a) HBsAg and unrelated analyte b) CRP and c) IgA for the immunosensor.

selectivity of the sensor. Figure 12 shows calibration plots corresponding to the resistance change (ΔR_{et}) with different concentrations of the target analyte (HBsAg) and contrast analyte (CRP or IgA). There is only a slight variation in the impedance with the increase of contrast analytes. Such small changes in R_{et} of the nonspecific adsorption are acceptable. This indicates that the observed changes of the electron transfer resistance with HBsAg were the specific antibody–antigen interaction, which made this immunosensor feasible for the determination of HBsAg in human specimens.

2.2.6. Precision, Reproducibility, and Stability of the Immunosensor

For each measurement, because EIS was performed when the diffusion layer had grown sufficiently, the immunosensor showed good reproducibility. The relative standard deviation (RSD) of five successive measurements to 0.1 pg mL^{-1} of HBsAg was 2.9%. The reproducibility of the immunosensor for HBsAg was investigated with intra- and interassay precision. The intra-assay precision of the immunosensor was evaluated by assaying one HBsAg level for three reduplicate measurements, whereas the interassay precision was estimated by measuring one HBsAg level with three immunosensors prepared independently at the same experimental conditions. The intra- and interassay variation coefficients obtained from 1.0 pg mL^{-1} HBsAg were 6.7% and 5.3%, respectively, indicating acceptable precision and fabrication reproducibility.

The immunosensor could retain its EIS and CV response after a storage period of 60 days in PBS (10 mM, pH 7.0) at 4 °C without obvious decline. It indicated that the 3DOM IL-PANI electrode prepared by the inverse-opal technique can provide a large active surface, which is efficient at retaining the bioactivity of antibody molecules. On the other hand, because of the covalent interaction between the L-Cys modified IL-PANI macroporous structure and primary amine groups in biomolecules, it could also prevent the biomolecules from leaking out. The regeneration of the immunosensor was developed by rinsing with stripping buffer of pH 2.8 Gly–HCl solution to dissociate the Ag–Ab complex. The as-renewed immunosensor could restore 92% of the initial value after five assay runs, showing high reusability and stability.

Table 1. Comparison of serum HBsAg levels determined using two methods.

Serum samples	Immunosensors [ng mL ⁻¹]	Commercial turbidimetric method	Relative deviation [%]
1	16.5 ± 0.2	17.5 ± 0.1	-5.7
2	44.3 ± 0.3	41.2 ± 0.2	7.5
3	102.4 ± 0.3	97.2 ± 0.5	5.3
4	168.0 ± 0.5	177.2 ± 0.2	-5.2
5	256.3 ± 0.4	243.7 ± 0.5	5.2

2.2.7. Application of the Immunosensor in Human Serum

The feasibility of the immunoassay system for clinical applications was investigated by analyzing several clinical samples in comparison with the commercial turbidimetric method performed in Nanjing Gulou Hospital. These serum samples were detected by an appropriate dilution with pH 7.0 PBS. The data of conditions, optimizations, and calibration curves were the average of three measurements. These results (Table 1) indicated that the presented method was in acceptable agreement with the traditional clinical method. Thus, the proposed method could satisfy the clinical need for immunoassays of HBsAg levels.

3. Conclusions

PANI inverse opals doped with IL have been successfully synthesized by electropolymerization, which is convenient, efficient, and rapid. The as-prepared inverse opals inherit excellent stability and conductivity, which facilitates the loading of AuNPs on the surface by self-assembly. The resulting AuNP/IL-PANI inverse opal hybrids have been used to fabricate a novel label-free electrochemical immunoassay for the detection of HBsAg based on a HBsAb/L-Cys/AuNP/IL-PANI hybrid material. This immunoassay is versatile, selective, and reproducible for protein analysis and this work demonstrates the potential application of the AuNP/IL-PANI inverse opals in the broad bioassay field.

4. Experimental

Chemicals: HBsAb (2.0 mg mL⁻¹) and HBsAg (2.0 mg mL⁻¹) were purchased from Shanghai YeMin Biological Technology Company (Shanghai, China). The monodisperse silica spheres with the diameters of 0.25, 0.5, and 1.0 μm were obtained from Alfa Aesar. Human serum samples were obtained from Nanjing Gulou Hospital and used as received. The real serum samples were diluted to the appropriate concentrations (0.001 to 100 pg mL⁻¹) with PBS. BMIm⁺BF₄⁻ (1-butyl-3-methylimidazolium tetrafluoroborate) (purity > 99%) were purchased from the Lanzhou Institute of Chemical Physics, Chinese Academy of Sciences and were dried in vacuum at 60 °C for 24 h and then stored in a desiccator before being used. HAuCl₄ · 4H₂O and trisodium citrate were obtained from Shanghai Reagent Company (Shanghai, China). L-Cysteine (L-Cys) was from BIO BASIC INC. 1-ethyl-3-(3-dimethylaminopropyl) carbodiimide hydrochloride (EDC), N-hydroxysuccinimide (NHS), and lyophilized 99% BSA were from Sigma-Aldrich. PBS (10 mM, pH 7.0) was prepared by varying the ratio of NaH₂PO₄ to Na₂HPO₄. The standard HBsAg solution was prepared in the PBS solution and HBsAb was stored at 4 °C. Aniline monomer was distilled under reduced pressure. Other reagents such as anhydrous ethanol, acetone, HCl, HF, K₃Fe(CN)₆, K₄Fe(CN)₆, and NaOH were of analytical

grade and used as received without any further treatment. Ultrapure fresh water obtained from a Millipore water purification system (MilliQ, specific resistivity > 18 MΩ cm⁻¹, S. A. Molsheim, France) was used throughout this work.

Apparatus: The morphology of the 3DOM IL-PANI inverse opal film was verified by field-emission SEM (FESEM, HITACHI S4800). AFM images were obtained on a SPI3800 controller operating in tapping mode with an acquisition frequency of 1.5 Hz and a line density of 512.2 × 2 μm scans. UV-Vis and diffuse reflectance spectra (DRS) were recorded on a Shimadzu UV-2401 recording spectrophotometer at room temperature. The static water contact angles were measured at 25 °C by a contact angle meter (Rame-Hart-100) using drops of pure deionized water. The readings were stabilized and taken within 120 s after the addition.

Electrochemical Measurements: The electropolymerization was performed on a CHI660B electrochemical analyzer (Co. CHI, USA) with a conventional three-electrode system composed of a platinum wire as the auxiliary electrode, a saturated calomel electrode (SCE) as the reference, and a gold substrate close-packed with 3D silica colloidal crystal as the working electrode. The geometric area of the working electrode was controlled by insulating tape covering the edges of SiO₂ layers and determined to be 0.07 cm². All the CV and EIS measurements were carried out on an Autolab PGSTAT12 (Eco chemie, BV, The Netherlands) and controlled by GPES 4.9 and FRA 4.9 software. All solutions were deoxygenated by highly pure nitrogen and kept in a nitrogen atmosphere in the measurements. The EIS measurements were recorded within the frequency range of 0.1–1.0 × 10⁵ Hz at the formal potential of the [Fe(CN)₆]^{3-/4-} redox couple and with a perturbation potential of 5 mV.

Preparation of Colloidal Crystal Template: The SiO₂ colloidal crystal templates were fabricated on Au substrates provided by the 55th Institute of China Electronic Group (Nanjing, China). The Au substrates were prepared by sputtering 200 nm Au onto the quartz wafers with a few nanometers of Cr adhesion layer in vacuum. Before being used, the Au substrates were rinsed by acetone, piranha solution, and anhydrous ethanol respectively, and then dried under nitrogen flow. After the pretreatment, the surfaces of the Au substrate became hydrophilic and were suitable for the self-assembly of SiO₂ spheres. The vertical deposition method was used to assemble SiO₂ spheres to the Au substrates by immersing one Au substrate vertically into about 15 mL SiO₂ colloidal suspension, which was dispersed by 0.30 g of SiO₂ spheres into 60 mL water/ethanol (90:10 v/v) mixture ultrasonically. This apparatus was covered by a 250 mL beaker or other suitable vessel and placed in a temperature-controlled vibration-free furnace chamber (35 °C) for 48 h, after which, along with the evaporation of solvents, a 3D colloidal crystal template was obtained.

Preparation of 3DOM IL-PANI Inverse Opals: The fabrication procedure of the 3DOM IL-PANI inverse opals by electropolymerization with the SiO₂ colloidal templates is shown in Scheme 1. After infiltration of aniline solution (0.5 M aniline in 1.0 M HCl, and 0.044 M BMIm⁺BF₄⁻) into the interstices of the colloidal template, electropolymerization was carried out by a potentiostatic technique at a potential of 0.65 V until the charge reached 0.01 C. After polymerization, the resulting film was thoroughly rinsed with 1.0 M HCl and then aqueous HF (5%) was used for 3 min to remove the SiO₂ spheres, forming the 3DOM IL-PANI inverse opals.

Fabrication of the Immunosensor: AuNPs were prepared according to the literature [57] in addition to a sodium citrate solution put into a boiling HAuCl₄ solution. After the preparation of the 3DOM IL-PANI inverse opal, it was firstly dipped in Au colloid solution for 9 h at 4 °C to form the AuNP/IL-PANI composite. The composite was then rinsed with PBS (pH 7.0) solution for three times and was subsequently dipped in 20 mM L-Cys aqueous solution for 20 h at 4 °C. After thoroughly rinsing with PBS solution to remove physically adsorbed L-Cys, it was immersed in a solution with 20 mg mL⁻¹ of EDC and 10 mg mL⁻¹ of NHS for 1 h at room temperature. After the activated electrode L-Cys/AuNP/IL-PANI was rinsed with PBS, it was soaked in 500 μg mL⁻¹ of HBsAb PBS solution overnight to yield sensing interfaces. Unbound antibodies were washed away by PBS. The unreacted covalent active surface groups were subsequently blocked with 3% (w/w) BSA at 37 °C for 1 h, followed by three careful PBS washes. The fabricated HBsAg immunosensor was stored at 4 °C when not in use.

Electrochemical Measurement: The HBsAg was incubated with 300 μL of detecting Ag samples for 40 min at 50 $^{\circ}\text{C}$. The electrodes were washed carefully with PBS solution to remove nonspecifically bound conjugates. The electrochemical measurements including CV and EIS were performed in a degassed PBS solution containing 5.0 mM $\text{K}_3\text{Fe}(\text{CN})_6/\text{K}_4\text{Fe}(\text{CN})_6$ (1:1) mixtures with 0.1 M KCl as a supporting electrolyte.

Acknowledgements

We greatly appreciate the support of the National Natural Science Foundation of China for the Key program (20635020), Creative Research Group (20821063), and General program (90606016, 20605011). This work is also supported by the National Basic Research Program of China (2006CB933201). The authors thank Prof. Kui Zhang from Nanjing Gulou Hospital for her kind help.

Received: June 6, 2009

Published online: August 26, 2009

- [1] P. Alivisatos, *Nat. Biotechnol.* **2004**, *22*, 47.
- [2] E. Katz, C. I. Willner, *Angew. Chem. Int. Ed.* **2004**, *43*, 6042.
- [3] N. L. Rosi, C. A. Mirkin, *Chem. Rev.* **2005**, *105*, 1547.
- [4] X. J. Chen, Y. Y. Wang, J. J. Zhou, W. Yan, X. H. Li, J. J. Zhu, *Anal. Chem.* **2008**, *80*, 2133.
- [5] Z. J. Yang, Z. Y. Xie, H. Liu, F. Yan, H. X. Ju, *Adv. Funct. Mater.* **2008**, *18*, 3991.
- [6] O. D. Velev, P. M. Tessier, A. M. Lenhoff, E. W. Kaler, *Nature* **1999**, *401*, 548.
- [7] P. Jiang, J. Cizeron, J. F. Bertone, V. L. Colvin, *J. Am. Chem. Soc.* **1999**, *121*, 7957.
- [8] H. F. Zhang, A. I. Cooper, *J. Mater. Chem.* **2005**, *15*, 2157.
- [9] H. W. Yang, C. F. Blanford, J. C. Lytle, C. B. Carter, W. H. Smyrl, A. Stein, *Chem. Mater.* **2001**, *13*, 4314.
- [10] C. Yue, T. Michel, D. Antonelli, *Chem. Commun.* **2006**, 1918.
- [11] M. A. Carreon, V. V. Gulians, *Eur. J. Inorg. Chem.* **2005**, 27.
- [12] P. Jiang, J. F. Bertone, V. L. Colvin, *Science* **2001**, *291*, 453.
- [13] Y. Jiang, X. M. Meng, J. Liu, Z. Y. Xie, C. S. Lee, S. T. Lee, *Adv. Mater.* **2003**, *15*, 323.
- [14] A. Rügge, J. S. Park, R. G. Gordon, S. H. Tolbert, *J. Phys. Chem. B* **2005**, *109*, 3764.
- [15] C. Wu, T. Bein, *Science* **1994**, *264*, 1757.
- [16] T. Cassagneau, F. Caruso, *Adv. Mater.* **2002**, *14*, 1629.
- [17] T. Cassagneau, F. Caruso, *Adv. Mater.* **2002**, *14*, 1837.
- [18] M. Deutsch, Y. A. Vlasov, D. J. Norris, *Adv. Mater.* **2000**, *12*, 1176.
- [19] T. Sumida, Y. Wada, T. Kitamura, S. Yanagida, *Chem. Commun.* **2000**, 1613.
- [20] S. H. Park, Y. Xia, *Adv. Mater.* **1998**, *10*, 1045.
- [21] S. A. Johnson, P. J. Oliver, T. E. Mallouk, *Science* **1999**, *283*, 963.
- [22] P. N. Bartlett, P. R. Birkin, M. A. Ghanem, C. S. Toh, *J. Mater. Chem.* **2001**, *11*, 849.
- [23] V. V. R. Sai, S. Mahajan, A. Q. Contractor, S. Mukherji, *Anal. Chem.* **2006**, *78*, 8368.
- [24] Y. Wang, F. Caruso, *Adv. Funct. Mater.* **2004**, *14*, 1012.
- [25] Y. Wang, F. Caruso, *Chem. Commun.* **2004**, 1528.
- [26] W. Qian, Z. Gu, A. Fujishima, O. Sato, *Langmuir* **2002**, *18*, 4526.
- [27] R. A. Barry, P. Wiltzius, *Langmuir* **2006**, *22*, 1369.
- [28] S. J. Tian, J. J. Wang, U. Jonas, W. Knoll, *Chem. Mater.* **2005**, *17*, 5726.
- [29] X. Luo, A. J. Killard, A. Morrin, M. R. Smyth, *Chem. Commun.* **2007**, 3207.
- [30] X. Luo, A. J. Killard, M. R. Smyth, *Chem. Eur. J.* **2007**, *13*, 2138.
- [31] X. Yang, Y. Jin, Y. Zhu, L. Tang, C. Li, *J. Electrochem. Soc.* **2008**, *155*, J23.
- [32] A. F. Diaz, J. A. Logan, *J. Electroanal. Chem.* **1980**, *111*, 111.
- [33] T. Ohsaka, Y. Ohnuki, N. Oyama, K. Katagiri, K. Kamisako, *J. Electroanal. Chem.* **1984**, *161*, 399.
- [34] O. A. Raitman, E. Katz, A. F. Buckmann, I. Willner, *J. Am. Chem. Soc.* **2002**, *124*, 6487.
- [35] S. J. Tian, N. R. Armstrong, W. Knoll, *Langmuir* **2005**, *21*, 4656.
- [36] S. J. Tian, A. Baba, J. Y. Liu, Z. H. Wang, W. Knoll, M. K. Park, R. Advincula, *Adv. Funct. Mater.* **2003**, *13*, 473.
- [37] A. Saheb, M. Josowicz, J. Janata, *Anal. Chem.* **2008**, *80*, 4214.
- [38] W. Yang, J. Liu, R. Zheng, Z. Liu, Y. Dai, D. Chen, S. Ringer, F. Braet, *Nanoscale Res. Lett.* **2008**, *3*, 468.
- [39] S. Mu, *J. Phys. Chem. B* **2008**, *112*, 6344.
- [40] Z. Zhou, D. He, X. Li, S. Wang, G. Li, *Polym. Sci. Ser. B* **2008**, *50*, 209.
- [41] T. Welton, *Chem. Rev.* **1999**, *99*, 2071.
- [42] L. Y. Yang, W. B. Liao, *Macromol. Chem. Phys.* **2007**, *208*, 994.
- [43] J. H. O. Owino, A. Ignaszak, A. Al-Ahmed, P. G. L. Baker, H. Alemu, J. C. Ngila, E. I. Iwuoha, *Anal. Bioanal. Chem.* **2007**, *388*, 1069.
- [44] T. Cassagneau, F. Caruso, *Adv. Mater.* **2002**, *14*, 34.
- [45] D. Wang, F. Caruso, *Adv. Mater.* **2001**, *13*, 350.
- [46] S. Q. Liu, D. Leech, H. X. Ju, *Anal. Lett.* **2003**, *36*, 1.
- [47] X. L. He, R. Yuan, Y. Q. Chai, Y. Zhang, Y. T. Shi, *Biotechnol. Lett.* **2007**, *29*, 149.
- [48] E. Katz, I. Willner, *Electroanalysis* **2003**, *15*, 913.
- [49] S. Hleli, C. Martelet, A. Abdelghani, F. Bessueille, A. Errachid, J. Samitier, H. C. W. Hays, P. A. Millner, N. Burais, N. Jaffrezic-Renault, *Mater. Sci. Eng. C* **2006**, *26*, 322.
- [50] W. Yan, X. J. Chen, X. H. Li, X. M. Feng, J. J. Zhu, *J. Phys. Chem. B* **2008**, *112*, 1275.
- [51] S. Zhang, F. Huang, B. Liu, J. Ding, X. Xu, J. Kong, *Talanta* **2007**, *71*, 874.
- [52] H. Tang, J. Chen, L. Nie, Y. Kuang, S. Yao, *Biosens. Bioelectron.* **2007**, *22*, 1061.
- [53] H. Huang, P. Ran, Z. Liu, *Bioelectrochemistry* **2007**, *70*, 257.
- [54] Y. S. Lee, B. K. Kim, E.-C. Choi, *Arch. Pharmacol. Res.* **1998**, *21*, 521.
- [55] D. Tleugabulova, V. Falcon, E. Penton, M. Sewer, Y. Fleitas, *J. Chromatogr. B* **1999**, *736*, 153.
- [56] S. Iyer, R. S. Robin Robinett, H. HogenEsch, S. L. Hem, *Vaccine* **2004**, *22*, 1475.
- [57] J. Turkevich, P. C. Stevenson, J. Hiller, *Discuss. Faraday Soc.* **1951**, *11*, 55.